HANDHELD ED-XRF ANALYSIS OF OBSIDIAN FROM THE CLASSIC MAYA CITY OF PALENQUE, CHIAPAS, MEXICO

Lucas R. Martindale Johnson,[a] Lisa M. Johnson,[b] Jordan Kobylt,[c] and Cheyenne Laux[c]

[a] Far Western Anthropological Research Group, Inc., Desert Branch, USA
[b] University of Nevada, Las Vegas, Department of Anthropology, USA
[c] University of California, Berkeley, Department of Anthropology, USA

Introduction

The Classic Period (250 – 900 A.D.) Maya city of Palenque is located on the Western border of the Maya cultural region, in what is today, Chiapas, Mexico. Following a century of excavations, epigraphy and art history, we understand Palenque as a powerful political center in the wider Maya region with far-reaching political, military, and economic ties. The core area of Palenque is roughly 2.2 square kilometers and made up of 1,500 mapped visible structures. The height of the city's occupation, reaching an estimated 4,147 – 6,220 was during the Late Classic period, between 600's and late 700's (Barnhart 2007). Much of the city's major monumental structures and a few elite residential structures immediately adjacent to these areas have been excavated by multiple archaeological projects. More recently, the Palenque Regional Project (PRP), has initiated intensive archaeological investigations within the city's residential sector to further our understanding of Palenque's social organization and life within the city. Included in that study is a series of analyses of excavated materials.

This report presents the results of a geochemical sourcing analysis of a small obsidian assemblage from an elite residential group, "Group IV." "Group IV" was the residence of a politically connected, and influential social group situated just 300 meters northeast of the city's palace compound. The residential group was composed of multiple structures enclosing a central patio space. Excavations in 2016 and 2017 were concentrated on two funerary structures within the residential group, structures J6 and J7 (Figure 1; see also Johnson 2018: 57, Figure 5). A series of carbon dates recovered from J7 on the eastern side of the patio group range between 534 – 710 CE or Late Classic Period. Structure J6, on the northeast corner produced a carbon date ranging from 768 – 905 CE or Terminal Classic Period (see Johnson 2018, Appendix 2). The obsidian that forms the basis of this study was recovered from primary contexts including burials and ritual deposits as well as secondary contexts, particularly the mixed matrix that made up the construction "fill" in both funerary shrines. Figure 2 shows a three-dimensional image of structure J7 with a buried altar exposed that is just beneath the latest construction phase.

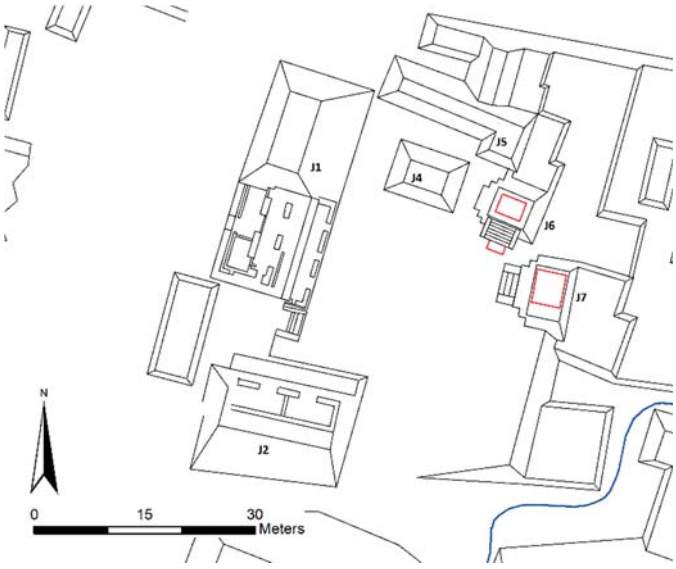

Figure 1. Overview of Group IV investigations. Note structures J6 and J7 are on the eastern side of the open central plaza (Arianna Campiani 2016, used with permission)

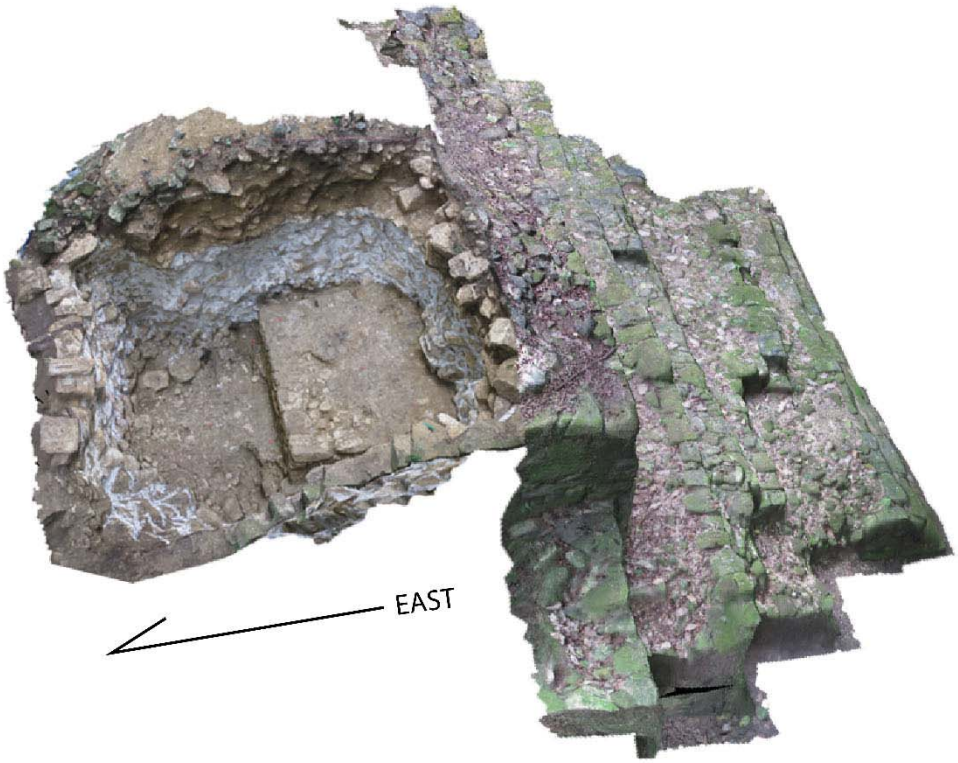

Figure 2. Three-dimensional overview of structure J7 during excavation. Note the buried central altar (Arianna Campiani 2016, used with permission).

Material and Methods

Analysis from two excavations included 189 artifacts. After initial inspection of the XRF spectra, one was determined to be a dark chert and is therefore not included in results. Cherts are easily identified during initial review of spectra; they exhibit no or very small peaks of trace elements common to obsidian spectra. If peaks are present among mid-z elements (i.e., Sr-Nb), they often equate to less than ten parts per million (ppm) for elements.

The artifacts include technological types common to Mesoamerican blade production. These include exhausted core fragments, core maintenance debitage, and used and unused blades, mostly medial fragments. Technological analysis followed those outlined by Kenneth Hirth (2006). Noteworthy here is that many of the blade specimens are relatively thin, 1-3 millimeters and thus are likely to provide lower count rates while using XRF (see below). These lower count rates often significantly alter the predicted ppm from common obsidian calibration methods (see Davis et al. 2011; Ferguson 2012 for discussions). Due to these limitations, we used other methods beyond ppm to source smaller and thinner artifacts following those procedures outlined by Richard Hughes (2010) and others where the use of ratioed net peak counts are useful as well as the use of peak percentages.

Assigning our modest sample to known obsidian sources in Mesoamerica was possible through comparison with a sample of geological source material. The element concentrations of the geological reference materials are summarized in Table 1. These

source references were generously provided by Mike Glascock and Jeff Ferguson from the University of Missouri Research Reactor (MURR) to Lucas Johnson as part of his dissertation research through the University of Florida and the Archaeological Research Facility (ARF) at the University of California Berkeley (see Johnson 2016).

Energy dispersive XRF (ED-XRF) analysis was conducted using a Bruker Tracer III-SD handheld XRF analyzer (Serial Number T3S1330) owned by the ARF. This XRF is equipped with a rhodium (Rh) X-ray tube and specimens were analyzed at 40 kV and 12.3 µA for 180 live seconds with a 10-square-millimeter XFlash® detector, using a "green" filter composed of six mils copper, one mil titanium, and 12 mils aluminum without a vacuum (Ferguson 2012:412). The resolution of the detector is approximately 145 eV at 200,000 counts per second. The X-ray beam focuses on an area of approximately two by three millimeters.

Each scan records intensities for the K-alpha peaks of manganese (Mn), iron (Fe), zinc (Zn), gallium (Ga), rubidium (Rb), strontium (Sr), yttrium (Y), zirconium (Zr), and niobium (Nb), and the L-alpha peaks of thorium (Th). Trace-element peak intensities for the these elements are normalized to the Compton scatter peak of rhodium (19.5–22 keV) and converted to ppm using the MURR 2 matrix-specific calibration, developed by Bruker Elemental, in collaboration with MURR (Glascock and Ferguson 2012; Speakman 2012). This factory-installed calibration is based on analysis of 40 samples of unmodified obsidian and fine-grained volcanic rock from around the world, chosen by Bruker and MURR to represent the range of trace-element concentrations known to occur in these materials. The USGS standard RGM-2, reported in Table 1, is not included in

		Elements (part per million)								
Chemical Group	N	Mn	Fe	Zn	Ga	Rb	Sr	Y	Zr	Nb
Cerro Varal	5	405±49	6987±471	41±6	19±3	128±5	74±6	23±1	121±8	17±1
El Chayal	5	603±115	6155±209	44±11	18±1	140±5	133±7	19±2	104±3	11±1
Fuentezuelas	5	206±75	14345±203	148±7	24±2	171±5	1±1	97±1	611±4	34±2
Ixtepeque	4	420±37	9149±257	44±4	21±1	100±2	146±8	18±1	161±7	10±1
La Union[1]	3	451±143	7920±434	47±7	18±1	130±12	38±6	24±4	141±6	16±3
Otumba	5	401±22	8866±364	50±7	19±2	124±5	118±6	22±1	136±3	12±1
Pachuca	5	1050±79	15709±181	208±5	23±1	195±2	4±0	109±3	891±3	88±1
Paredon	5	364±28	8777±316	62±2	22±2	165±7	4±1	48±3	201±9	41±2
San Martin	5	553±28	6510±153	47±3	18±1	109±4	172±4	15±2	110±3	9±1
Tulancingo	5	436±47	18443±706	186±13	24±2	126±5	13±1	93±5	685±31	46±1
Ucareo	5	208±17	7569±120	44±9	19±1	150±6	10±1	26±1	115±3	14±1
Zacualtipan	5	184±26	10584±552	48±4	23±2	282±9	36±2	46±2	213±5	19±1
Zaragoza	5	263±29	9595±343	46±6	22±1	138±5	26±2	32±2	189±8	17±1
RGM-2 Measured	13	269±39	12066±431	38±7	16±3	130±13	87±10	23±2	186±19	9±1
RGM-2 Recommended[2]	1	273±8	13008±273	33±2	16±1	147±5	108±5	24±2	222±17	9±0

Note – [1] UC Berkeley Source, all others are provided by MURR; [2] USGS RGM-2 (Wilson 2009)

Table 1. Source library summary and analysis of USGS RGM-2 pressed pellet analyzed with Bruker Tracer III-SD ED-XRF serial number T3S1330

SUMMARY DATA	ELEMENTS IN CALIBRATION (PPM)									
	Mn	Fe	Zn	Ga	Th	Rb	Sr	Y	Zr	Nb
Minimum	172	3,690	27	12	1	11	0	15	60	2
Maximum	1,775	68,537	592	32	83	436	291	415	3,066	640
Average	571	14,150	101	20	18	160	59	63	391	65
Calibration Error	25	248	4	3	1	3	1	2	4	2
r^{2a}	0.99	0.99	0.99	0.35	0.98	0.99	0.99	0.99	1.0	0.99
Slope[b]	1.0	1.0	1.0	0.92	1.0	0.97	1.0	1.0	1.0	1.0

Notes: [a] Calculated predicted ppm values to known ppm values (Glascock and Ferguson 2012).
r^2 – Coefficient of determination. [b] a measurement of accuracy comparing known values to predicted.

Table 2. Calibration Ranges and Associated Statistics of MURR 2 Calibration by Element (concentrations in parts per million).

the MURR 2 calibration. Minimum and maximum values for element regression lines used for this analysis and other statistics associated with the MURR 2 calibration standards, as it pertains to serial number T3S1878, are shown in Table 2.

To accommodate analysis of small artifacts, trace element values are presented in three ways: as concentrations in parts per million, and as peak ratios and relative percentages. The latter facilitate interpretation of results for artifacts that are smaller than the two-by-three-millimeter incident X-ray beam, or thinner than "infinite thickness", that is, the sample thickness required to absorb all incoming X-rays. For the analytical conditions used here, infinite thickness in an obsidian matrix is approximately four millimeters. For artifacts less than four millimeters thick, a portion of the incoming X-rays will escape through the back of the sample, resulting in a lower than normal signal for a given trace element in a particular obsidian (Ferguson 2012: Figure 12.4). Normalization to the Compton scatter peak of rhodium, as described above, corrects ppm concentrations for this effect down to a specimen thickness of approximately 1.5 millimeters and a diameter of four millimeters (Davis et al. 2011), but distortion in ppm values for specimens below this threshold is often considerable. For these specimens, relative peak intensities or peak ratios are used to make source assignments in addition to parts per million (Hughes 2010), as these values are typically more stable with diminishing artifact size and thickness. Small artifacts are also compared to 95% confidence regions calculated from the non-Euclidean Mahalanobis Distance statistic (see Hamilton 2018).

Results

Multivariate trace-element analysis determined the presence of just two sources of obsidian among the two archaeological investigations at Palenque's Group IV. El Chayal obsidian accounts for 185 artifacts and Zaragoza is represented by just three specimens (Table 3). While this sample size is biased to just two excavations, the results do support reports of both Guatemalan and Mexican obsidian sources. Flavio G. Silvia de la Mora (2018) demonstrates the overwhelming presence of El Chayal obsidian (n=1,293) in the sites east of Palenque. Zaragoza obsidian is present (n=9) as well as other Mexican obsidian (see Silva de la Mora 2018, 492-495). These results are similar to another study conducted at the site of Palenque conducted by Jay Johnson (1976).

The current Group IV sample shows that core-sized materials were imported into the site as represented by two exhausted cores that accord with El Chayal source materials. The

					El Chayal (parts per million)									
			Counts per second		*Rb*		*Sr*		*Y*		*Zr*		*Nb*	
Type	Subtype	n=	Mean	COV	Mean	COV	Mean	COV	Mean	COV	Mean	COV	Mean	COV
Blade	Final series	148	1032±163	16	163±11	7	155±11	7	21±2	10	117±6	5	12±1	11
Blade	Initial series	19	1174±213	18	161±14	9	153±11	7	21±1	6	117±5	5	12±1	10
Blade	Macro Blade	1	1314±0	-	155±0	-	143±0	-	19±0	-	109±0	-	10±0	-
Core	Exhausted Core	2	1615±24	1	132±2	2	128±1	1	19±1	4	102±1	1	11±1	7
Flake	Core Tablet	1	1544±0	-	141±0	-	135±0	-	20±0	-	111±0	-	10±0	-
Flake	Distal Core Rejuvenation	1	1538±0	-	136±0	-	134±0	-	22±0	-	105±0	-	11±0	-
Flake	Macro Flake	4	1191±171	14	157±9	6	146±9	6	20±1	7	117±5	4	12±2	17
Flake	Overhang Removal	2	1219±75	6	155±17	11	146±9	6	20±1	7	116±4	3	11±3	26
Flake	Small Percussion Debitage	1	1088±0	-	150±0	-	142±0	-	19±0	-	113±0	-	13±0	-
Flake	Other	1	1362±0	-	144±0	-	138±0	-	19±0	-	111±0	-	12±	-
Other	Undiagnostic	5	711±137	19	167±6	4	161±7	4	19±1	7	114±5	5	11±1	13
	Subtotal	185												
					Zaragoza (parts per million)									
Blade	Final series	2	1217±6	1	150±7	5	27±0	0	35±3	8	197±1	1	20±1	7
Blade	Initial series	1	1542±0	-	137±0	-	26±0	-	32±0	-	185±0	-	19±0	-
	Subtotal	3												

Table 3. Handheld portable XRF element concentration summary of artifacts grouped by source assignment and technology. Note, individual artifact geochemistry is available upon request.

Zaragoza material is represented by just three blades. Technological analyses are important variables to consider in obsidian sourcing as it relates directly with overall artifact morphology and more importantly to XRF fluorescence efficiency. While cores are blocky and often exceed the minimum thickness and diameter (4x4x4 millimeters) to generate sufficient counting statistics for XRF, blades often return far fewer counts (see Ferguson 2012, 415 Figure 12.4). For example, the source reference material returns count rates per second of 1,240-1,781, while the artifacts returned count rates per second of 532-1,632. Table 3 also show count rates per second by artifact type and source. The lower XRF count rates are associated with those artifacts that are thinner or smaller in diameter (see blades and undiagnostic debitage). These lower counts do distort ppm predictions (Davis et al. 2011). Figure 3 demonstrates the distortion in strontium with many of the samples plotting far outside the 95% confidence ellipse for El Chayal obsidian. Other semi-quantitative methods are therefore employed for resolving these seemingly outliers.

Semi-quantitative methods include the transformation or manipulation of cumulative element photon counts but can include ratio transformations of ppm data (see Frahm 2016). In this analysis we make use of photon count data and do not transform predicted ppm data. Photon ratio transformations demonstrate less distortion in the ppm element concentrations (Table 4 and Figure 4). The use of element ratio data helps to normalize distortion from artifact morphology. Source assignments using ratio data can also be supported by the use of photon

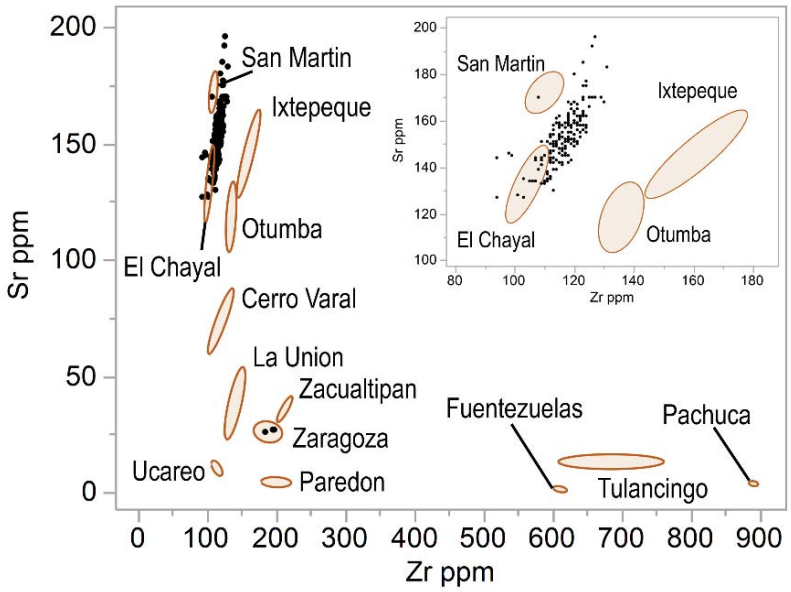

Figure 3. Zr by Sr biplot of all artifacts with obsidian sources represented by 95% confidence ellipses. Note the elevated concentration (i.e., ppm over estimation) of Sr due to thinness of many blade artifacts (see inset).

peak intensity percentages (Hughes 2010), which sums the cumulative counts for three elements (Rb, Sr and Zr) and then calculates their respective percentage of this sum (i.e., 0-100%). Data are displayed using ternary diagrams (Figure 5). While outliers still exist for both semi-quantitative approaches, they do resolve the significant strontium over-estimation shown in Figure 3 and eliminate other possible overlaps with alternative obsidian sources.

Discussion and Conclusion

While our modest obsidian study is not robust to determine site wide obsidian exchange or use patterns, we do introduce data that supports a more regional analysis (Silva de la Mora 2018; Johnson 1976). The analysis shows El Chayal obsidian continues to be the dominate source for obsidian in the Classic period regardless of regional occupation within the Maya Lowlands (see also Johnson 2016; Moholy-Nagy 2013). The next phase of

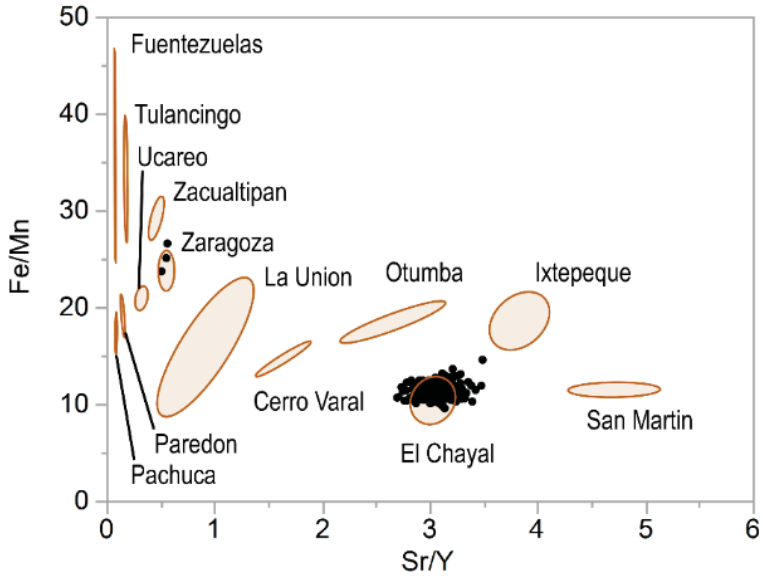

Figure 4. Fe/Mn by Sr/Y peak intensity ratio biplot with geological reference samples represented by 95% confidence ellipses.

	Sources	∑Rb.Sr.Zr	Rb%	Sr%	Zr%	Fe/Mn	Rb/Sr	Zr/Y	Y/Nb	Zr/Nb	Sr/Y
Artifacts	El Chayal	6816 ±835	0.30 ±0.01	0.34 ±0.01	0.35 ±0.01	11.28 ±0.77	0.88 ±0.03	3.16 ±0.16	1.67 ±0.1	5.28 ±0.34	3.08 ±0.15
	Zaragoza	7164 ±105	0.31 ±0.01	0.08 ±0.01	0.61 ±0.01	25.10 ±1.44	3.67 ±0.15	3.92 ±0.17	1.52 ±0.05	5.95 ±0.26	0.54 ±0.03
Source References	El Chayal	7627 ±340	0.30 ±0.01	0.34 ±0.01	0.36 ±0	10.35 ±1.01	0.88 ±0.03	3.16 ±0.1	1.59 ±0.08	5.03 ±0.1	3.03 ±0.09
	Fuentezuelas	17478 ±179	0.16 ±0.01	0.01 ±0	0.83 ±0	35.62 ±4.43	13.65 ±0.73	5.77 ±0.05	2.10 ±0.06	12.13 ±0.43	0.08 ±0
	Ixtepeque	8285 ±290	0.19 ±0.01	0.33 ±0.01	0.48 ±0.01	18.56 ±1.22	0.58 ±0.02	5.61 ±0.15	1.45 ±0.05	8.13 0.27	3.83 ±0.11
	La Union	6605 ±381	0.33 ±0.01	0.13 ±0.01	0.53 ±0.02	15.86 ±2.93	2.49 ±0.21	3.62 ±0.36	1.37 ±0.03	4.96 ±0.59	0.92 ±0.18
	Otumba	7730 ±239	0.26 ±0.01	0.30 ±0.01	0.44 ±0	18.44 ±0.89	0.87 ±0.05	3.94 ±0.15	1.50 ±0.08	5.90 ±0.25	2.66 ±0.2
	Pachuca	24428 ±313	0.13 ±0.01	0.01 ±0	0.86 ±0	17.27 ±0.89	12.20 ±0.59	7.49 ±0.17	1.12 ±0.03	8.37 ±0.06	0.09 ±0
	Paredon	7608 ±195	0.35 ±0	0.03 ±0	0.63 ±0.01	19.07 ±0.95	11.45 ±0.65	3.12 ±0.12	1.14 ±0.04	3.56 ±0.09	0.15 ±0.01
	San Martin	8284 ±391	0.22 ±0	0.41 ±0	0.37 ±0.01	11.45 ±0.32	0.54 ±0.01	4.19 ±0.19	1.45 ±0.09	6.10 ±0.43	4.71 ±0.17
	Tulancingo	18046 ±790	0.11 ±0	0.02 ±0	0.87 ±0.01	33.21 ±2.69	4.87 ±0.28	7.07 ±0.39	1.57 ±0.03	11.11 ±0.62	0.18 ±0.01
	Ucareo	5625 ±133	0.45 ±0.01	0.06 ±0	0.49 ±0.01	20.90 ±0.51	7.31 ±0.47	2.59 ±0.03	1.63 ±0.05	4.23 ±0.17	0.32 ±0.02
	Zacualtipan	10317 ±75	0.43 ±0.01	0.08 ±0	0.49 ±0	29.16 ±0.93	5.41 ±0.3	2.86 ±0.12	2.25 ±0.12	6.44 ±0.38	0.46 ±0.03
	Zaragoza	7231 ±160	0.30 ±0	0.08± 0.01	0.61± 0.01	23.74 ±0.85	3.59 ±0.18	4.05 ±0.16	1.55 ±0.03	6.27 ±0.25	0.56 ±0.03

Table 4. Photon count ratios and peak count percentages for artifacts by source assignments and source reference materials provided by MURR and UC Berkeley.

obsidian research at Palenque plans to gather samples from those residences around Group IV as part of a neighborhood investigation carried out by the Palenque Regional Project (PRP).

Furthermore, the obsidian study shows how artifact morphology may create problems in obsidian sourcing. Small and thin artifacts do not generate similar XRF counting statistics like those of more robust samples, including source library references that meet or exceed four millimeters. The use of other methods, often termed "semi-quantitative", require extracting photon count data from element spectra. These peak intensity measures are available through various XRF manufacturers'

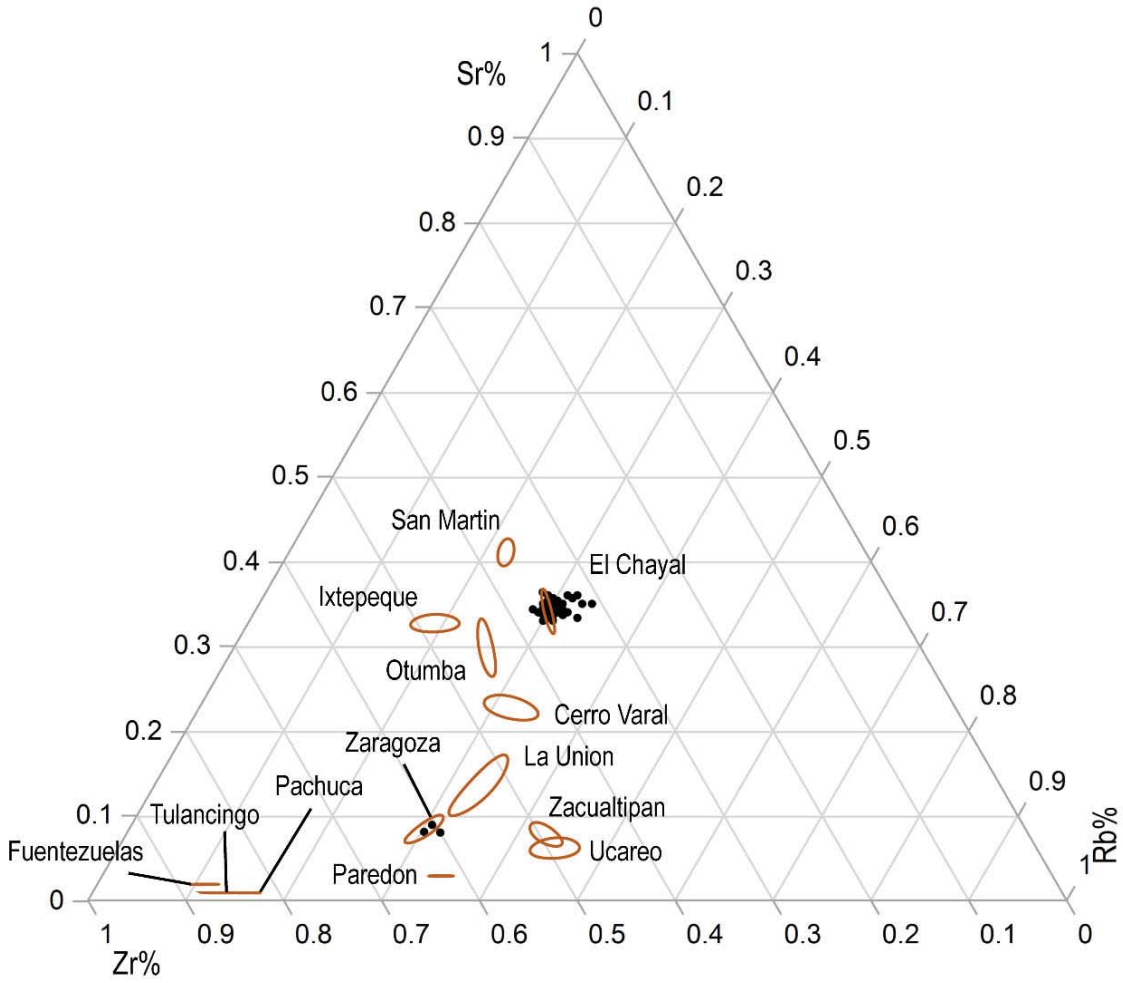

Figure 5. Ternary plot using peak intensity percentages for all artifacts with 95% confidence regions for obsidian reference samples. Note, confidence regions are constructed in R using the package ggtern that uses the Mahalanobis non-Euclidian distance statistic (see Hamilton 2018; R Core Team; Johnson et al. 2018 for a discussion).

software. Bruker's is typically extracted from calibration worksheets or other software, whereas Olympus' is a selected export within the general export functions. It is advisable to curate both ppm and photon count data, including overall count rates, as part of an obsidian study. With the growth of XRF use, these varied measures of element concentration help to further data transparency.

Acknowledgments

These data were collected and analyzed with the help of Rosemary Joyce and Nicholas Tripcevich of the Archaeological Research Facility at the University of California Berkeley. Rodrigo Liendo from the Universidad de Nacional Autónoma de México, Instituto de Investigaciones Antropológicas is the project permit holder and supervised the excavations. Mike Glascock and Jeff Ferguson of the University of Missouri Research Reactor provided obsidian source reference materials and Nickolas Hamilton, the creator of ggtern for R, instructed in the use of open-source coding. This research was made possible through funding from a UC MEXUS Dissertation Research Grant DI-15-7 and Wenner Gren Dissertation Grant #9543

References Cited

Barnhart, E. (2007) Indicators of Urbanism at Palenque. In *Palenque: Recent Investigations at the Classic Maya Center,* edited by D. Marken, pp. 107 – 121. Alta Mira Press, Lanham.

Davis, M. K., T. L. Jackson, M. S. Shackley, T. Teague, and J. H. Hampel (2011) Factors Affecting the Energy-Dispersive X-Ray Fluorescence (EDXRF) Analysis of Archaeological Obsidian. In *X-Ray Fluorescence Spectrometry (XRF) in Geoarchaeology*, edited by M. S. Shackley, pp. 45-64. Springer, New York

Ferguson, J. (2012) X-Ray Fluorescence of Obsidian: Approaches to Calibration and the Analysis of Small Samples. In *Studies in Archaeological Sciences: Handheld XRF for Art and Archaeology,* edited by A. N. Shugar and J. L. Mass, pp. 401-422. Leuven University Press, Belgium.

Frahm, E. (2016) Can I Get Chips with That? Sourcing Small Obsidian Artifacts Down to Microdebitage Scales with Portable XRF. *Journal of Archaeological Sciences: Reports* 9: 448-467.

Glascock, M., and J. Ferguson (2012) *Report on the Analysis of Obsidian Source Samples by Multiple Analytical Methods*. Unpublished manuscript. Archaeometry Laboratory, University of Missouri Research Reactor.

Hamilton, N. (2018) ggtern: An Extension to 'ggplot2', for the Creation of Ternary Diagrams. R package v. 2.2.2. https://CRAN.R-project.org/package=ggtern

Hirth, K. G. [editor] (2006) *Obsidian Craft Production in Ancient Central America: Archaeological Research at Xochicalco.* University of Utah Press, Salt Lake City.

Hughes, R. E. (2010) Determining the Geologic Provenance of Tiny Obsidian Flakes in Archaeology Using Nondestructive EDXRF. *American Laboratory* 42(7): 27-31.

Johnson, J. K. (1976) Long Distance Obsidian Trade: New Data from the Western Maya Periphery. In *Maya Lithic Studies: Papers from the 1976 Belize Field Symposium,* edited by T. R. Hester and N. Hammond, pp. 83 – 90. Center for Archaeological Research, University of Texas, San Antonio.

Johnson, L. M. (2018) *Tracing the Ritual 'Event' at the Classic Maya City of Palenque, Mexico.* Unpublished Ph.D. Dissertation, Department of Anthropology, University of California, Berkeley.

Johnson, L. R. M. (2016) *Toward an Itinerary of Stone: Investigating the Movement, Crafting, and Use of Obsidian from Caracol, Belize.* Unpublished Ph.D. Dissertation, Department of Anthropology, University of Florida.

Johnson, L. R. M., M. Badillo, N. Hamilton, and S. Batty (2018) Reporting on an Additional Obsidian Macro-core from Belize, Central America: Morphology, Geochemistry, and Significance. *IAOS Bulletin* 59: 19-27.

Moholy-Nagy, H., J. Meierhoff, M. Golitko, and C. Kestle (2013) An Analysis of pXRF Obsidian Source Attributions from Tikal, Guatemala. *Latin American Antiquity* 24(1): 72-97.

de la Mora, F. G. S. (2018) Obsidian Procurement and Distribution in the Northwestern Maya Lowlands during the Maya Classic, a Regional Perspective. *Journal of Archaeological Science: Reports* 18: 577-586.

R Core Team (2018) R: A language and Environment for Statistical Computing. R Foundation for Statistical Computing, Vienna, Austria. http://www.R-project.org/.

Speakman, R. J. (2012) *Evaluation of Bruker's Tracer Family Factory Obsidian Calibration for Handheld Portable XRF Studies of Obsidian*. Prepared for Bruker AXS, Kennewick, Washington.

Wilson, S. (2009) *Certificate of Analysis: Rhyolite, Glass Mountain RGM-2*. United States Geological Survey. https://crustal.usgs.gov/geochemical_reference_standards/pdfs/RGM-2.pdf, accessed October 2017.